JOURNAL OF MOLECULAR RECOGNITION
J. Mol. Recognit. 2007; **20**: 516–523
Published online 8 October 2007 in Wiley InterScience
(www.interscience.wiley.com) DOI:10.1002/jmr.848

Force microscopy imaging of individual protein molecules with sub-pico Newton force sensitivity

Shivprasad Patil, Nicolas F. Martinez, Jose R. Lozano and Ricardo Garcia*
Instituto de Microelectrónica de Madrid, CSIC, Isaac Newton 8, 28760 Tres Cantos, Madrid, Spain

The capability of atomic force microscopes (AFM) to generate atomic or nanoscale resolution images of surfaces has deeply transformed the study of materials. However, high resolution imaging of biological systems has proved more difficult than obtaining atomic resolution images of crystalline surfaces. In many cases, the forces exerted by the tip on the molecules (1–10 nN) either displace them laterally or break the noncovalent bonds that hold the biomolecules together. Here, we apply a force microscope concept based on the simultaneous excitation of the first two flexural modes of the cantilever. The coupling of the modes generated by the tip–molecule forces enables imaging under the application of forces (∼35 pN) which are smaller than those needed to break noncovalent bonds. With this instrument we have resolved the intramolecular structure of antibodies in monomer and pentameric forms. Furthermore, the instrument has a force sensitivity of 0.2 pN which enables the identification of compositional changes along the protein fragments. Copyright © 2007 John Wiley & Sons, Ltd.

Keywords: **atomic force microscopy; picoNewton forces; antibodies; flexural modes; nonlinear dynamics; IgG; IgM**

Received 19 June 2007; revised 2 August 2007; accepted 3 August 2007

INTRODUCTION

Progress on spatial resolution has driven the evolution of force microscopy from static to dynamic excitation modes (Bustamante and Keller, 1996; Engel and Müller, 2000; San Paulo and Garcia, 2000; Hörber and Miles, 2003; Hinterdorfer and Dufrene, 2006). In all the cases, the improvement of the spatial resolution was accompanied by a reduction of the normal and lateral forces exerted by the tip on the surface. However, achieving molecular resolution images of biological systems has been much more difficult than obtaining atomic resolution images of crystalline surfaces (Ohnesorge and Binnig, 1993; Klinov and Magonov, 2004; Giessibl and Quate, 2006). In most of the cases, the forces exerted by the tip on the molecules (1–10 nN) either displace them laterally or break the noncovalent bonds that held the biomolecules together (Fritz *et al*., 1995; San Paulo and Garcia, 2000; Pignataro *et al*., 2002; Moreno-Herrero *et al*., 2003; Solares, 2007), which in turn prevents high resolution imaging. The individual noncovalent bonds that hold together the tertiary structure of proteins (∼50 pN) may be broken by the AFM probe. Furthermore, protein unfolding requires forces in the 50–100 pN range. These facts have prevented the observation by AFM of individual biomolecules in a true non-invasive manner.

Typical AFM images of individual proteins either in air or in solution are hard to interpret because they show featureless globular structures. Several attempts have rendered images of individual protein (Hafner *et al*., 1999; San Paulo and Garcia, 2000; Kienberger *et al*., 2004; Stroh *et al*., 2004). The substructure of immunoglobulin G was resolved to 25 kDa by amplitude modulation AFM (AM-AFM) in air (Thomson, 2005). However, those experiments implied the application of forces above 200 pN, which either introduced unwanted modification on the molecules or limited the spatial resolution to about 4 nm.

On the other hand, molecular resolution images have been achieved by imaging crystalline or semicrystalline two dimensional protein or lipid bilayer domains in liquid (Engel and Müller, 2000; Ando *et al*., 2001; Scheuring *et al*., 2003, 2004; Higgins *et al*., 2006; Hoogenboom *et al*., 2006; Yokokawa *et al*., 2006). In these situations, the close packing of molecules provided a mechanism to release the force exerted by the tip into vertical and lateral elastic deformations, so that the molecular shape remains unchanged during imaging. Additionally, periodic structures make it possible to use statistical analysis to improve resolution (Engel and Müller, 2000).

Recent approaches to improve spatial and/or compositional resolution by force microscopy have either been focused on reducing the deflection detection noise (Fukuma *et al*., 2005) which enabled the use of very small amplitudes (∼0.1 nm) or the use of higher harmonics (Sahin *et al*., 2004; Stark, 2004; Legleiter *et al*., 2006) to enhance the sensitivity to tip–surface interactions. In particular, theoretical modelling has shown that in the presence of mode coupling (Rodriguez and Garcia, 2004), the second flexural mode of the cantilever could be more sensitive to tip–surface force while minimizing surface deformation. Experimental results have confirmed the validity of the above simulations for mechanical (Martinez *et al*., 2006;

*Correspondence to: R. Garcia, Instituto de Microelectrónica de Madrid, CSIC, Isaac Newton 8, 28760 Tres Cantos, Madrid, Spain.
E-mail: rgarcia@imm.cnm.csic.es

Proksch, 2006) and electrostatic interactions (Stark *et al*., 2007).

In this study, we demonstrate that the spatial contrast and force sensitivity of an atomic force microscope (AFM) while imaging individual biomolecules can be improved by operating the instrument at lower forces. This is achieved by operating the AFM under the simultaneous excitation of the first two cantilever modes. The root mean square (rms) amplitude of the first mode is used as the feedback parameter while the phase shift of the second mode is used to obtain compositional maps with very high force sensitivities. The tip–molecule forces generate higher harmonics of the first mode. Whenever the frequency of a higher harmonic matches or is close to the frequency of the second mode (here, $f_2 = 6.2 f_1 \approx n f_1$, with $n = 6$) the modes became coupled. This coupling is substantially enhanced by the initial non-zero amplitude of the second mode which leads to operate the AFM at larger tip–molecule separations, i.e. under very small forces.

MATERIALS AND METHODS

Force microscopy

The experiments were performed in air at a relative humidity of 40% with a modified AM-AFM that enables the simultaneous excitation of the first and second resonances of the microcantilever (Martinez *et al*., 2006). The bi-modal AFM excitation force is

$$F_{\text{ext}}(x,t) = F_1 \cos \omega_1 t + F_2 \cos \omega_2 t \qquad (1)$$

where ω_1 and ω_2 are the angular frequencies of the first and second resonances respectively (Figure 1A and B). The phase and amplitude of both modes are measured independently by using two quadrature circuits. The rms amplitude of the first mode is fed back to the controller for conventional topography imaging while the phase shifts of the second mode are recorded and plotted to obtain compositional maps. Imaging has been performed with free amplitudes in the range of 5–25 nm and 0.2–1 nm for the first and second mode respectively (A_{01} and A_{02}). The feedback loop actuates on the amplitude of the first mode and it is set approximately at $0.9A_{01}$. The tip was scanned across the surface at 1 Hz. Topography and compositional images were obtained with rectangular silicon cantilevers with nominal tip radii of 2–5 nm, force constants about 10 N/m and resonance frequency about 120 kHz (SEIHR, Nanosensors, Germany). The noise level in the force sensor for the bi-modal AFM is 70 pm/$\sqrt{\text{Hz}}$.

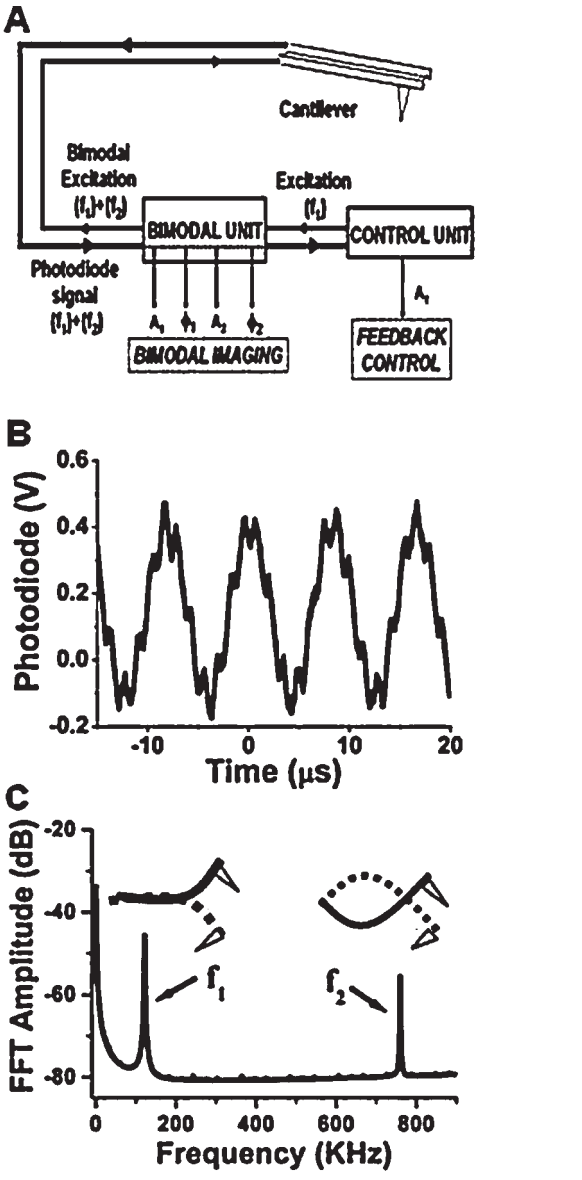

Figure 1. (A) Electronic signal routing in bi-modal AFM operation. (B) Photodiode signal under bi-modal AFM operation. (C) The fast Fourier transform shows the first two flexural modes, $f_1 = 120.35$ kHz and $f_2 = 760.08$ KHz.

Antibodies

Monoclonal IgG antibodies (Ab 38C2, Sigma) samples were prepared from a stock solution of 1 mg/μl by diluting to 10 μg/ml in distilled water. A drop of 10 μl was deposited for 30 s on a freshly cleaved mica surface, rinsed in distilled water and dried with N gas. Pentameric IgM samples were prepared from purified human IgM (Sigma) by diluting the original solution 1:100 in distilled water. A drop of 10 μl was deposited for 45 s on a freshly cleaved mica surface, rinsed in distilled water and dried with N gas.

Dynamic AFM simulations

In AM-AFM there is no practical experimental protocol to measure instantaneous forces and to determine force sensitivities. This is in contrast with respect to contact AFM. Nonetheless, numerical simulations could be used to determine the forces. The simulations are performed by modelling the three dimensional microcantilever as a rectangular beam and applying the Euler–Bernoulli equation

DOI: 10.1002/jmr

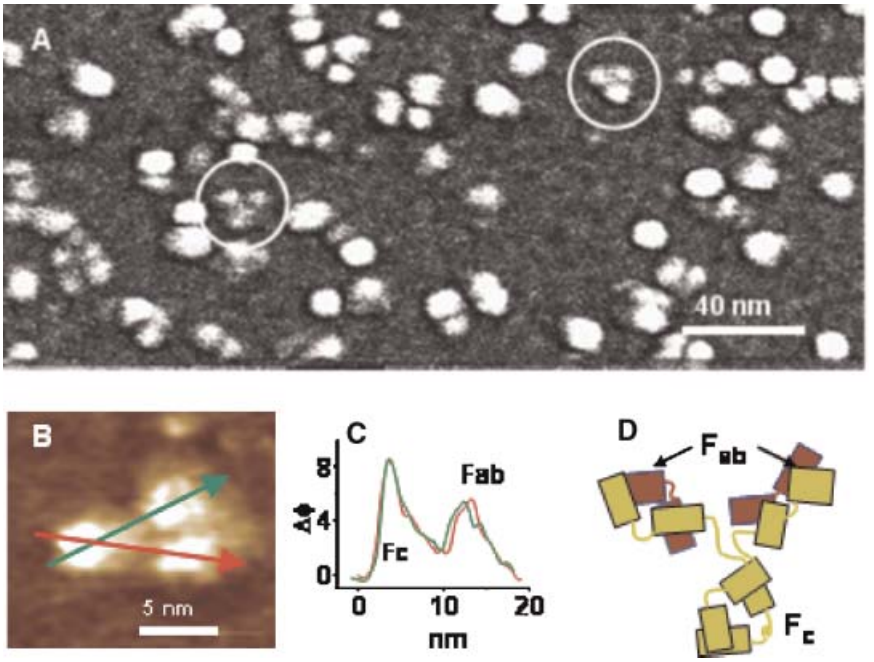

Figure 2. (A) Bi-modal AFM phase image of a mica surface with physisorbed with IgG monomers ($A_{01} = 23$ nm, $A_{02} = 0.4$ nm). (B) Image of an individual antibody. (C) Phase shift cross sections along the arrows depicted in Figure 2B. (D) Schematic of the tertiary structure of IgG molecules. The heavy chains are in green and the light chains in red (adapted from Thomson, 2005). This figure is available in colour online at www.interscience.wiley.com/journal/jmr

(Rodriguez and Garcia, 2002). We also consider that the continuous beam is excited under the bi-modal regime. The model only considers long-range attractive forces between tip and sample surface. The results of the simulations are compared with experimental phase versus separation curves. The good qualitative and quantitative agreement between theory and experiments allows us to estimate the force sensitivity under the experimental conditions described here.

EXPERIMENTAL RESULTS

Antibodies are proteins that have well defined structures (Hafner *et al*., 1999; Alberts *et al*., 2002; Kienberger *et al*., 2004) and binding sites (Kienberger *et al*., 2004) which make them good candidates to test the sensitivity and resolution of the bi-modal AFM for biomolecular imaging. Immunoglubulin G (IgG) is a Y-shaped protein that consists of four polypeptide chains arranged in three fragments, one Fc receptor and two identical Fab antigen-binding sites (Figure 2D). The van der Waals length of each fragment is about 6.5 nm. Because of the flexibility of IgG, the antibody adopts several morphologies and in particular the Y shape.

We have used the bi-modal AFM to image small and flexible IgG antibodies deposited on mica. Figure 2A shows a second mode phase image of IgG antibodies, in particular two of them have the Y-shaped morphology. It has been shown before that the antibodies can adopt different orientations on the support (San Paulo and Garcia, 2000; Kienberger *et al*., 2004). Figure 2B shows an individual antibody with Y-shaped orientation with all its fragments accessible to AFM image analysis. The cross-section along the lines depicted in Figure 2B allows us to identify the position of the Fc and Fab fragments (Figure 2C). Two of the fragments show the same phase shift of 5° while the third fragment shows a phase shift at 8° (Figure 2C). The phase shifts are relative to the mica surface. This result where the phase shift on the molecule shows three peaks, two of them are identical and smaller in value than the other, has also been found on other IgG molecules. Consequently, we assign the largest peak to the Fc fragment and the smaller peaks to the Fab fragments. The result indicates that the identification of different components along the protein chains is possible by the present method.

We have also imaged complex protein structures such as immunoglobulin M pentamers (IgM) (Figure 3A). IgM has five Ig monomers, each of them having one Fc and two Fab fragments. Additionally there is a small polypeptide chain (J-chain) joining two consecutive Fc fragments. The image shows several IgM molecules together with smaller structures that could be detached fragments of IgM. The pentagonal shape and the position of the J-chain (central structure) are readily recognized in high resolution bi-modal phase images (Figure. 3B–D). We have measured the angles between the lines joining the J-chain and two consecutive monomers. The histogram shows a single and dominant peak centred at 70°, i.e. very close to the theoretical value of 72° for a rigid pentamer (Figure 3E). The above difference as well as the slightly distorted pentagonal structure observed in Figure 3B–D are attributed to the flexible character of the

DOI: 10.1002/jmr

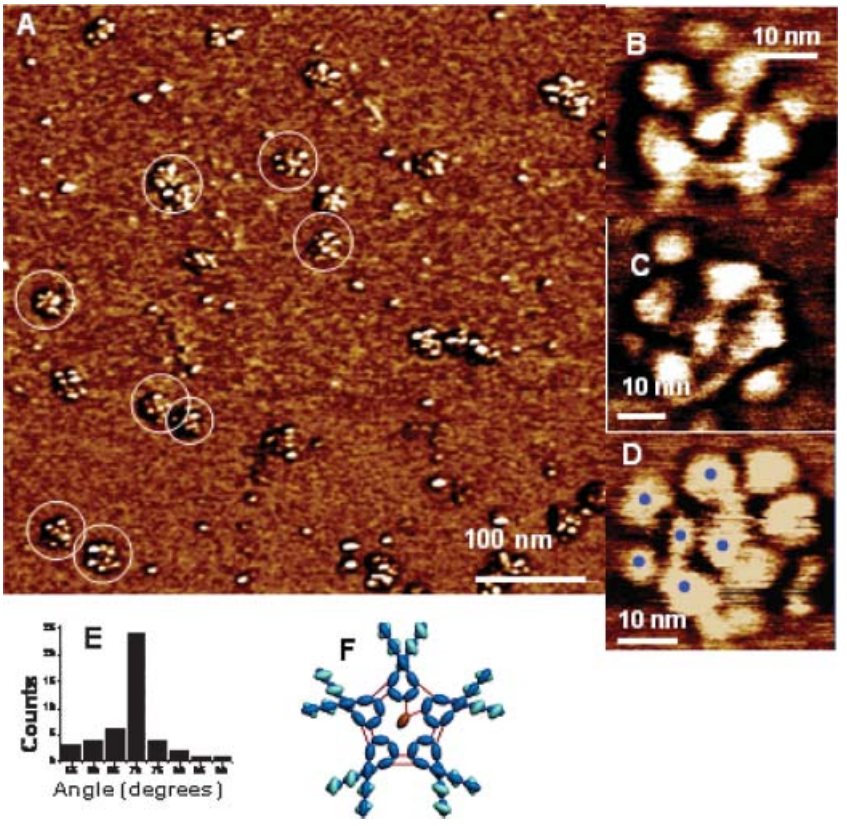

Figure 3. (A) Bi-modal AFM phase image of mica surface with physisorbed IgM pentamers. The image represents the variation of the phase shift of the second mode across the sample surface. (B), (C) and (D) Individual bi-modal AFM images show five subunits and a central structure (J-chain). (E) Statistical distribution of angles between the subunits of the pentamer, taken from bi-modal AFM images of individual IgM molecules. (F) Model of IgM. Light and solid blue represent light and heavy chains respectively; the J-chain appears in brown. Experiments were performed in air (relative humidity (RH) = 40%) with a cantilever with $f_1 = 118.8$ kHz, and $f_2 = 739.5$ kHz, $A_{01} = 22$ nm, and $A_{02} = 0.5$ nm.

Fab fragments. Previously, the only AFM images of IgM that hinted its pentagonal structure were obtained by using sharp carbon nanotube probes (Hafner *et al*., 1999).

A direct comparison between amplitude modulation (tapping mode) and bi-modal AFM images illustrates some of the advantages of the latter for high resolution imaging of isolated biomolecules under the application of very small forces. To assure a meaningful comparison, we have used an AFM that enables to perform both amplitude modulation and bi-modal AFM imaging with the same cantilevers. Figure 4A and B show tapping mode topography and phase shift image of an IgM antibody. The image was obtained by applying a maximum tip–molecule force below 100 pN. The small value of the force explains the lack of contrast in both AM-AFM images (see discussion below). Figure 4C shows the bi-modal AFM phase image obtained along with Figure 4A and B. The bi-modal AFM image shows the five Ig monomers as well as the J-chain. Similar results have been obtained by imaging IgG molecules. Tapping mode AFM images of a single IgG in both topography and phase shift (Figure 4D and E) show a featureless and faint object while the bi-modal AFM image resolves the Fab and Fc fragments of the protein (Figure 4F).

The spatial resolution in probe microscopy is defined as the minimum separation between two objects for which the dimple depth is larger than the instrumental noise (Bustamante and Keller, 1996). This criterion applied to Figures 2 and 3 where Fc, Fab, J-chain and hinge regions are resolved, gives a resolution of 1.5 nm.

THEORETICAL SIMULATIONS

The force sensitivity under bi-modal AFM operation is estimated by numerical simulations. The simulations are performed by modelling the three dimensional cantilever with a rectangular beam and solving the Euler–Bernoulli equation of motion under bi-modal excitation (Rodriguez and Garcia, 2004). The dynamic deflection function $w(x,t)$ of the cantilever follows

$$\frac{EI}{L^4}\frac{\partial^4}{\partial x^4}\left[w(x,t)+a_1\frac{\partial w(x,t)}{\partial t}\right]+bh\rho_c\frac{\partial^2 w(x,t)}{\partial t^2}=F(x,t) \quad (2)$$

DOI: 10.1002/jmr

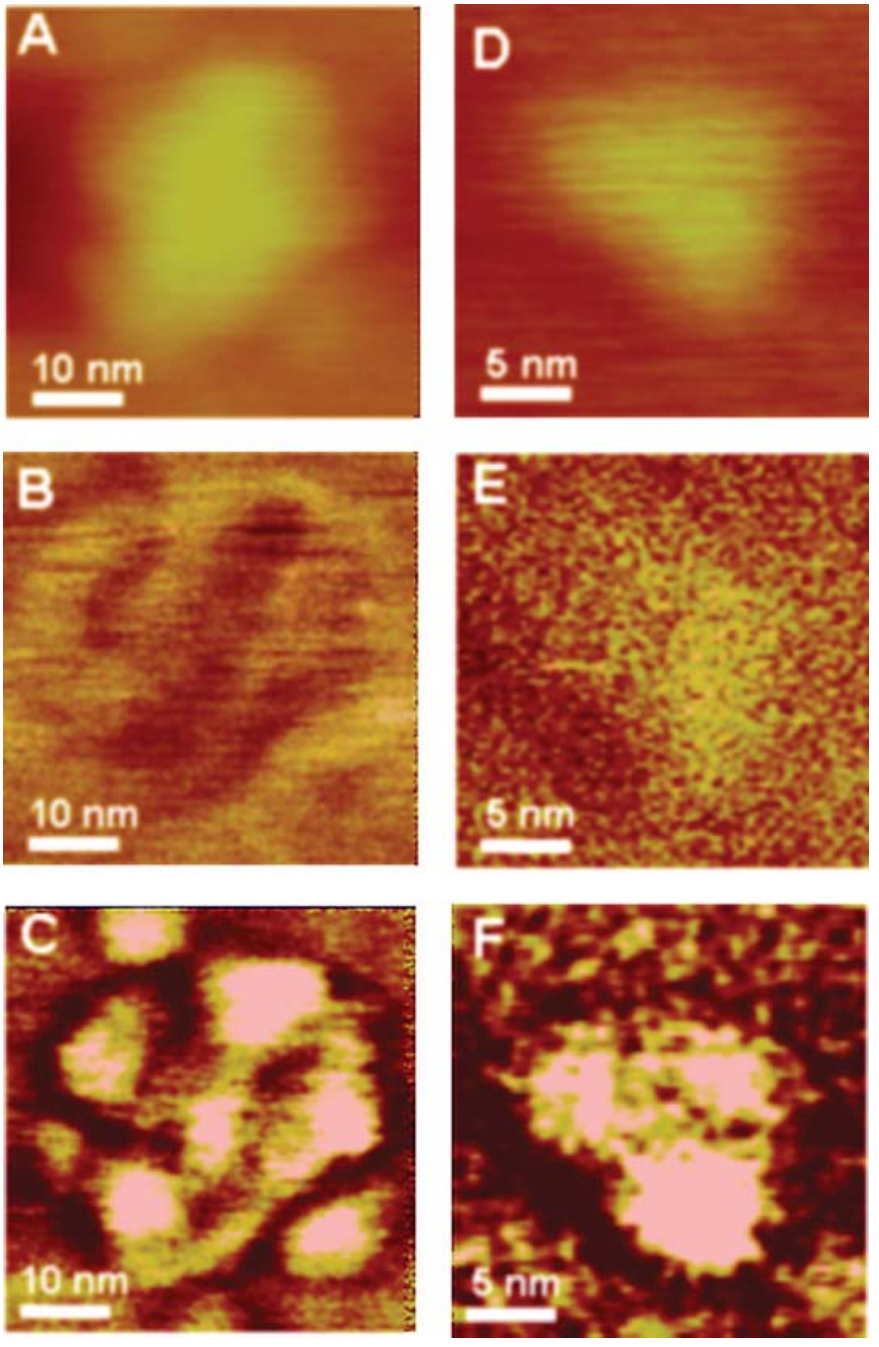

Figure 4. (A) Amplitude modulation AFM image (tapping mode) of IgM molecule (topography). (B) Amplitude modulation phase shift image of (A). (C) Bi-modal AFM phase image of the same IgM pentamer. The image shows the five subunits and the central structure (J-chain). Figure 4A–C have been obtained simultaneously. (D) Amplitude-modulation AFM topography image of an IgG molecule. (E) Phase shift image corresponding to (D). (F) Bi-modal AFM phase image of the same IgG. The image reveals the presence of Fab and Fc fragments. Figure 4D–F have been obtained simultaneously ($A_{01} = 23$ nm, $A_{02} = 0.4$ nm).

where x is the normalized coordinate along the beam and L the cantilever length; b and h are the width and thickness while E is the Young modulus, I the moment of inertia, ρ_c is the mass density and a_1 is the internal damping of the cantilever. The boundary conditions assume one end of the cantilever clamped and the other free. The relevant forces, expressed in the above equation in units of force per length, are the external excitation, hydrodynamic damping with the medium and tip–sample interaction forces respectively:

$$F(x,t) = F_{\text{ext}}(x,t) + F_{\text{med}}(x,t) + F_{\text{ts}}(x,t) \qquad (3)$$

The excitation force includes first and second mode components (see Equation 1). The model might include both

DOI: 10.1002/jmr

conservative long and short-range forces. However, we are mostly interested in the operation of the AFM in the non-contact regime, i.e. when the tip performs the full cycle without mechanical contact with the sample surface. Consequently, we simplify the calculations by using attractive forces of the type,

$$F_{ts}(X = L) = -\frac{\alpha}{d^2} \tag{4}$$

where α represents the strength of the interaction. In particular, for van der Waals forces the strength of the interaction can be expressed by $\alpha = HR/6$, where H is the Hamaker constant and R the effective interaction radius. The time-dependence of the Euler–Bernoulli equation was solved numerically by using a fourth-order Runge–Kutta algorithm.

Figure 5A shows the dependence of the second mode phase shift with respect to the oscillation amplitude (which is equivalent to the average tip–surface distance). The experiment is performed by approaching the vibrating tip towards the mica surface from a distance (mean value) several times larger than the free amplitude A_0. The experimental curve shows three regions, two regions characterized by high slopes at separations of $(0.7–1)A_0$ and $(0–0.15)A_0$ respectively, and a transition region with a nearly constant slope between 0.16 and $0.7A_0$. The quantitative agreement obtained between experiment and theory supports the validity of the model to describe bi-modal AFM operation. The above agreement allows us to calculate the force exerted by the tip on the sample and the force sensitivity of the second mode phase signal by fitting of experimental data to simulations. We remark that in AM-AFM there are no direct experimental measurements of the maximum force exerted on the sample.

The maximum force (F_{max}) exerted by the probe on the molecule is calculated by using the range of parameters for which a good fit between theory and experiments exists. Figure 5B shows the dependence of the F_{max} on the amplitude ratio. The force curve depends on the initial free amplitudes (filled circles $A_0 = 24$ nm versus open circles $A_0 = 6$ nm). For relevant experimental values ($A_0 \in$[5 and 20 nm] and $A_0/A \in$[0.8 and 1]), the force varies between 1 and 100 pN. For small free amplitudes (open circles) the force initially increases by decreasing the amplitude, and then it flattens out. At smaller amplitude ratios it increases again. The experimental phase shift profile of the second mode shown in Figure 2 D gives a maximum phase shift of 7°. The simulations show that the above phase shift profile involves maximum forces in the 35–38 pN range (Figure 5C). From the above curve, we obtain an approximate value of the slope $\approx$0.7 pN/degree. For a bandwidth of 3 kHz (imaging bandwidth) the noise in the phase signal is $\Delta\phi \sim 0.3°$ which translates into δF$\sim$0.2 pN, i.e. about two orders of magnitude smaller than previously reported by any AFM at the same bandwidth.

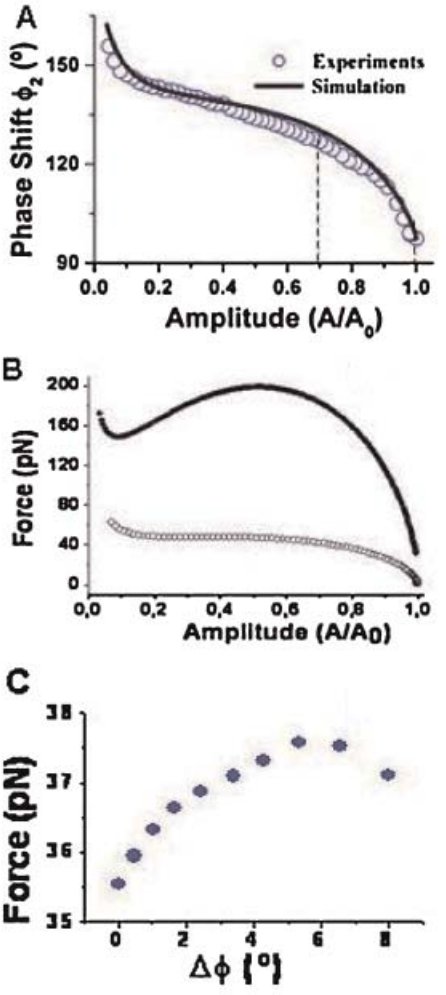

Figure 5. (A) Dependence of the phase shift of the second mode on the amplitude ratio on a mica surface. Dots represent experimental results and the continuous line is obtained from numerical simulation. $A_{01} = 24$ nm, $A_{02} = 0.4$ nm, $f_1 = 118.61$ kHz and $f_2 = 737.32$ kHz. (B) Calculated maximum force per cycle exerted on the mica surface for $A_{01} = 17$ nm, $A_{02} = 0.6$ nm, $R = 20$ nm (filled circles) and $A_{01} = 6$ nm, $A_{02} = 0.5$ nm and $R = 5$ nm (open circles). For mica a Hamaker constant of 9.03×10^{-20} J was used. (C) Calculated maximum force per cycle along the phase shift cross-sections shown in Figure 2C. The force corresponds to the different Hamaker values for the same tip radius and set point amplitudes. Hamaker constant values are (from the left to right) 9, 8, 7, 6, 5, 4, 3.5 and 3×10^{-20} J; $A_{01} = 6$ nm, $A_{02} = 0.5$ nm, $R = 5$ nm, $f_1 = 119.4$ kHz and $f_2 = 749.3$ kHz, $Q_1 = 255$ and $Q_2 = 1000$. This figure is available in colour online at www.interscience.wiley.com/journal/jmr

DISCUSSION AND CONCLUSIONS

The enhanced sensitivity obtained by the bi-modal AFM is a consequence of the nonlinear coupling of the first two flexural resonances, the higher sensitivity of the second mode with respect to the first, the use of phase shifts instead of amplitudes to detect forces and because we have decoupled microscopy operation from force detection. In AM-AFM operation, average tip–surface force and contrast are intrinsically linked by the expression (San Paulo and Garcia, 2001),

$$\langle F_{ts} \rangle = \frac{k}{2Q}[A_0^2 - A^2]^{1/2} \tag{5}$$

DOI: 10.1002/jmr

where k and Q are respectively the static force constant and the quality factor of the fundamental mode (first resonance). The typical tapping mode operation parameters are $k = 20$–50 N/m, $A_0 = 5$–10 nm, $A = 0.7\ A_0$ and Q is approximately 200. Substituting those values in Equation 5 yields the average tip–sample force to be in the range 100–900 pN. In bi-modal AFM, the first mode tracks the topography in exactly the same way as in AM-AFM. Equation 5 for the experimental parameters used in Figures 2–4 gives an average tip–sample force of 190 pN ($A = 0.9\ A_0$). That force is higher than the forces given by solving Equation 1 ($\sim$50 pN). The latter difference could be traced back to the fact that the point-mass model used to derive Equation 5 cannot capture the existence of higher eigenmodes. The tip–surface adhesion forces prevent the use of smaller free amplitudes. Thus, to operate the microscope under smaller forces will require the set-point amplitudes very close to A_0. This in turn implies to withdraw the tip with the subsequent reduction of the signal to noise ratio and loss of spatial resolution (see for example tapping AFM images taken at $0.9A_0$ in Figure 4B and E). Bi-modal AFM overcomes the above limitation by using the second mode as an additional interaction channel. The nonlinear coupling between first and second mode makes the latter extremely sensitive to short and long-range tip–surface interactions because it has both a higher quality factor ($Q_2 = 5Q_1$) and a higher optical sensitivity in beam deflection detectors ($\sim$4:1). Furthermore, the amplitude of the second mode is very small ($A_{02} \approx 0.5$ nm) which enables this mode to explore the relevant range of the interaction potential. In addition, the feedback loop does not actuate on the amplitude of the second mode so its phase shift instantly responds to minute tip–molecule force variations.

In summary, we have resolved the intramolecular structure of antibodies in monomer and pentameric forms by using a force microscope concept that involves the simultaneous excitation of its first two eigenmodes. We have demonstrated that under the same conditions, bi-modal AFM gives higher spatial contrast and resolution than tapping mode AFM. We have also demonstrated that bi-modal AFM allows to perform imaging in air under the application of maximum forces below 100 pN. We have estimated that the force sensitivity of this force microscopy mode is 0.2 pN. Finally, we conclude that the identification of the protein subunits based on measurements which are directly related to the strength of the tip–surface forces and thus to the chemical composition would enable this technique to image large protein complexes with true non-invasive forces.

Acknowledgments

This work was financially supported by the European Commission (FORCETOOL, NMP4-CT-2004-013684) and the Ministerio de Educación y Ciencia (MAT2006-03833).

REFERENCES

Alberts B, Johnson A, Lewis J, Raff M, Roberts K, Walter P. 2002. Molecular Biology of the Cell (4th edn). Garlang Science: New York.

Ando T, Kodera N, Takai E, Maruyama D, Saito K, Toda A. 2001. A high-speed atomic force microscope for studying biological macromolecules. *Proc. Natl Acad. Sci. USA* **98**: 12468–12472.

Bustamante C, Keller D. 1996. Scanning force microscopy in biology. *Phys. Today* **48**: 32–38.

Engel A, Müller DJ. 2000. Observing single biomolecules at work with the atomic force microscope. *Nat. Struct. Biol.* **7**: 715–718.

Fukuma T, Kobayashi K, Matsushige K, Yamada H. 2005. True molecular resolution in liquid by frequency modulation atomic force microscopy. *Appl. Phys. Lett.* **86**: 193108–193110.

Fritz M, Radmacher M, Cleveland JP, Allersma MW, Stewart RJ, Gieselmann R, Janmey P, Schmidt CF, Hansma PK. 1995. Imaging globular and filamentous proteins in physiological buffer solutions with tapping mode AFM. *Langmuir* **11**: 3529–3535.

Giessibl FJ, Quate CF. 2006. Exploring the nanoworld with the atomic force microscopy. *Phys. Today* **59**: 44–50.

Hafner JH, Cheung CL, Lieber CM. 1999. Growth of nanotubes for probe microscopy tips. *Nature* **398**: 762–763.

Higgins MJ, Polcik M, Fukuma T, Sader JE, Nakayama Y, Jarvis SP. 2006. Structured water layers adjacent to biological membranes. *Biophys. J.* **91**: 2532–2542.

Hörber JKH, Miles MJ. 2003. Scanning probe evolution in biology. *Science* **302**: 1002–1005.

Hinterdorfer P, Dufrene YF. 2006. Detection and localization of single molecular recognition events using atomic force microscopy. *Nat. Methods* **3**: 347–355.

Hoogenboom BW, Hug HJ, Pellmont Y, Martin S, Frederix PLTM, Fotiadis D, Engel A. 2006. Quantitative dynamic-mode scanning microscopy in liquid. *Appl. Phys. Lett.* **88**: 193109–193111.

Kienberger F, Mueller H, Pustushenko V, Hinterdorfer P. 2004. Following single antibody binding to purple membranes in real time. *EMBO Rep.* **5**: 579–583.

Klinov D, Magonov S. 2004. True molecular resolution in tapping mode atomic force microscopy with high resolution probes. *Appl. Phys. Lett.* **84**: 2697–2699.

Legleiter J, Park M, Cusik B, Kowalewski T. 2006. Scanning probe acceleration microscopy in fluids: mapping mechanical properties of surfaces at the nanoscale. *Proc. Natl Acad. Sci. USA* **103**: 4813–4818.

Martinez NF, Patil S, Lozano JR, Garcia R. 2006. Enhanced compositional sensitivity in atomic force microscopy by the excitation of first two flexural modes. *Appl. Phys. Lett.* **89**: 153115–153117.

Moreno-Herrero F, Colchero J, Baro AM. 2003. DNA height in scanning force microscopy. *Ultramicroscopy* **96**: 167–174.

Ohnesorge F, Binnig G. 1993. True atomic resolution by atomic force microscopy through repulsive and attractive forces. *Science* **260**: 1451–1456.

Pignataro B, Chi L, Gao S, Anczykowski B, Niemeyer C, Adler M, Fuchs H. 2002. Dynamic scanning force microscopy study of self-assembled DNA-protein nanostructures. *Appl. Phys. A* **74**: 447–452.

Proksch R. 2006. Multi-frequency, repulsive mode amplitude modulated atomic force microscopy. *Appl. Phys. Lett.* **89**: 113121–113123.

Rodriguez TR, Garcia R. 2004. Compositional mapping of surfaces in atomic force microscopy by excitation of the second normal mode of the microcantilever. *Appl. Phys. Lett.* **84**: 449–451.

DOI: 10.1002/jmr

Rodriguez TR, Garcia R. 2002. Tip-motion in amplitude modulation AFM: comparison between continuous and point-mass models. *Appl. Phys. Lett.* **80**: 1646–1648.

Sahin O, Quate CF, Solgaard O, Atalar A. 2004. Resonant harmonic response in tapping-mode atomic force microscopy. *Phys. Rev. B* **69**: 165416.

San Paulo A, Garcia R. 2000. High-resolution imaging of antibodies by tapping-mode AFM: attractive and repulsive tip-sample interactions regimes. *Biophys. J.* **78**: 1599–1605.

San Paulo A, Garcia R. 2001. Tip-surface forces, amplitude, and energy dissipation in amplitude-modulation force microscopy. *Phys. Rev. B* **64**: 193411.

Scheuring S, Seguin J, Marco S, Prima V, Bernadac A, Levy D, Rigaud JL. 2003. Nanodissection and high resolution imaging of the Rhodopseudomonas viridis photosynthetic core complex in native membranes by AFM. *Proc. Natl Acad. Sci. USA* **100**: 1690–1693.

Scheuring S, Rigaud JL, Sturgis JN. 2004. Variable LH2 stoichiometry and core clustering in native membranes of Rhodospirillum photometricum. *EMBO J.* **23**: 4127–4133.

Solares SD. 2007. Single biomolecule imaging with frequency and force modulation in tapping-mode AFM. *J. Phys. Chem. B* **111**: 2125–2129.

Stark RW. 2004. Spectroscopy of higher harmonics in dynamic atomic force microscopy. *Nanotechnology* **15**: 347–351.

Stark RW, Naujoks N, Stemmer A. 2007. Multifrequency electrostatic force microscopy in repulsive regime. *Nanotechnology* **18**: 065502.

Stroh C, Wang H, Bash R, Ashcroft B, Nelso J, Gruber H, Lohr D, Lindsay SM, Hinterdorfer P. 2004. Single-molecule recognition imaging microscopy. *Proc. Natl Acad. Sci. USA* **101**: 12503–12507.

Thomson NH. 2005. The substructure of immunoglobulin G resolved to 25 kDA using amplitude modulation in air. *Ultramicroscopy* **105**: 1003–1110.

Yokokawa M, Wada C, Ando T, Sakai N, Yagi A, Yoshimura SH, Takeyasu K. 2006. Fast-scanning AFM reveals the ATP/ADOP-dependent conformational changes of GroEL. *EMBO J.* **25**: 4567–4576.

DOI: 10.1002/jmr